Performance and Emission Investigations of Jatropha and Karanja Biodiesels in a Single-Cylinder Compression-Ignition Engine Using Endoscopic Imaging

Gayatri K. Mistri
Department of Mechanical & Industrial Engineering,
University of Illinois at Chicago,
Chicago, IL 60607

Suresh K. Aggarwal[1]
Department of Mechanical & Industrial Engineering,
University of Illinois at Chicago,
Chicago, IL 60607
e-mail: ska@uic.edu

Douglas Longman
Engine Combustion Research,
Argonne National Laboratory,
Lemont, IL 60439

Avinash K. Agarwal
Department of Mechanical Engineering,
Indian Institute of Technology, Kanpur,
Kanpur 208016, India

Biofuels produced from nonedible sources that are cultivated on marginal lands represent a viable source of renewable and carbon-neutral energy. In this context, biodiesel obtained from Jatropha and Karanja oil seeds have received significant interest, especially in South Asian subcontinent. Both of these fuels are produced from nonedible plant seeds with high oil content, which can be grown on marginal lands. In this research, we have investigated the performance and emission characteristics of Jatropha and Karanja methyl esters (biodiesel) and their blends with diesel. Another objective is to examine the effect of long-term storage on biodiesel's oxidative stability. The biodiesels were produced at Indian Institute of Technology Kanpur, (IIT Kanpur), India, and the engine experiments were performed in a single cylinder, four-stroke, compression ignition engine at Argonne National Laboratory (ANL), Chicago. An endoscope was used to visualize in-cylinder combustion events and examine the soot distribution. The effects of fuel and start of injection (SOI) on engine performance and emissions were investigated. Results indicated that ignition delay was shorter with biodiesel. Consequently, the cylinder pressure and premixed heat release were higher for diesel compared to biodiesel. Engine performance data for biodiesel (J100, K100) and biodiesel blends (J30, K30) showed an increase in brake thermal efficiency (BTE) (10.9%, 7.6% for biodiesel and blend, respectively), brake specific fuel consumption (BSFC) (13.1% and 5.6%), and nitrogen oxides (NOx) emission (9.8% and 12.9%), and a reduction in brake specific hydrocarbon emission (BSHC) (8.64% and 12.9%), and brake specific CO emission (BSCO) (15.56% and 4.0%). The soot analysis from optical images qualitatively showed that biodiesel and blends produced less soot compared to diesel. The temperature profiles obtained from optical imaging further supported higher NOx in biodiesels and their blends compared to diesel. Additionally, the data indicated that retarding the injection timing leads to higher BSFC, but lower flame temperatures and NOx levels along with higher soot formation for all test fuels. The physicochemical properties such as fatty acid profile, cetane number, and oxygen content in biodiesels support the observed combustion and emission characteristics of the fuels tested in this study. Finally, the effect of long-term storage is found to increase the glycerol content, acid value, and cetane number of the two biodiesels, indicating some oxidation of unsaturated fatty acids in the fuels.
[DOI: 10.1115/1.4031317]

1 Introduction

Biodiesel fuels produced from the transesterification of edible and nonedible sources have attracted significant interest due to their potential as a renewable and environmentally friendly fuel, especially for the transportation sector. These fuels are considered carbon-neutral since the agriculture feedstock used for producing them consumes significant amounts of CO_2 that is emitted from the combustion of these fuels. Moreover, they have other desirable properties, such as higher lubricity, low sulfur content, low toxicity, and miscible with conventional diesel fuels, implying that they can be used as blends within the existing infrastructure for fuel delivery and transport. Numerous engine and flame studies [1–6] have demonstrated their superior emission characteristics compared to the conventional diesel in terms of emissions of CO, unburned hydrocarbons (HC), and particulate matter, although NOx emission is generally increased in case of biodiesels. In spite of these advantages, the so-called first-generation biodiesels produced from edible agriculture crops are not considered a sustainable option due to concerns about deforestation and biodiversity, and the "food versus fuel" debate. On the other hand, the "second-generation" biofuels produced from nonedible sources [7–9], especially those cultivated on marginal and waste lands, have

[1]Corresponding author.

Contributed by the Internal Combustion Engine Division of ASME for publication in the Journal of Energy Resources Technology. Manuscript received April 26, 2015; final manuscript received July 30, 2015; published online September 7, 2015. Editor: Hameed Metghalchi.

significant potential to be a viable energy source. These include both gaseous fuels, such as syngas and biogas produced from various biomass and waste feedstock, and liquid fuels, which include Fischer–Tropsch fuels, bio-alcohols, and biodiesels produced from nonedible plant oils, such as Jatropha, Karanja, Mahua, Castor, Neem, etc.

Amongst the various nonedible oils, Jatropha perhaps has been used most extensively in biodiesel synthesis [9–11]. The Jatropha (*Jatropha Curcas*) plant has a short gestation period, high oil content, and can be cultivated in tropical and subtropical climates across the world. It also has high degree of resistance to aridity, and thus can also be grown in deserts. Karanja (*Pongamia Pinnata*) oil is another promising feedstock for biodiesel production. Its tree is native to the Indian subcontinent, but is now grown all over the world. There have been a number of experimental studies during the last two decades dealing with the production and utilization of biodiesel produced from Jatropha, Karanja, and other oils [10–19]. A variety of engines have been employed to investigate the performance and emission characteristics of these fuels. Both 100% biodiesel and their blends with diesel have been tested by varying various engine parameters, such as engine speed, load, fuel injection pressure, SOI, etc. While there have been some conflicting results regarding the effect of biodiesels on engine performance and emissions, most studies have reported shortened ignition delay, increased peak heat release rate (HRR) (H_{max}), reduction in CO, unburned HC and smoke, and increase in NOx emissions. Regarding engine performance, Ganapathy et al. [16] observed higher BTE with biodiesel compared to diesel at advanced SOI, but lower BTE as SOI was retarded. In contrast, Dhar and Agarwal [17] reported higher BTE with Karanaja biodiesel at various operating conditions, such as injection pressure, SOI, etc. This was attributed to more complete combustion in the case of biodiesel, which was consistent with the lower CO and HC emissions observed with biodiesel. They also reported an increase in the BSFC with biodiesel due to its lower heating value. Some conflicting data have also been reported regarding CO and HC emissions depending upon operating conditions. For instance, Sahoo and Das [15] observed both increased and decreased CO and HC emissions from biodiesel depending upon the blending ratio and other operating conditions.

The objective of this research is to investigate the combustion, performance, and emission characteristics of two biodiesels, namely, Jatropha (J100) and Karanja (K100) and their blends with diesel, and to present a comparative analysis with conventional diesel. In this collaborative work, the biodiesels were produced at IIT Kanpur, India, and the engine experiments were performed at ANL, IL. Tests are conducted at three different SOIs (−5 deg, −1 deg, and 3 deg ATDC) with a Caterpillar 3401 single cylinder, four-stroke, compression ignition engine using J100, K100, J30, K30 (30% biodiesel: 70% diesel by volume), and baseline conventional diesel. Other parameters, such as the fuel quantity per injection (100 mm^3), injection pressure (1584 bar), engine speed (1500 rpm), compression ratio (16.3:1), and EGR (0%) were kept fixed for all experiments. The effects of various fuels at different SOIs were characterized in terms of ignition delay, cylinder pressure (P), and HRR versus crank angle (CA), indicated mean effective pressure (IMEP), BTE, and BSFC. The raw emissions were converted to mass emissions and they are reported as BSCO, BSHC, and BSNOx. In addition, using an endoscope (AVL Visioscope), 2D images were obtained by visualizing the combustion process and these images were analyzed to reveal the temperature and soot distribution during combustion.

Another objective is to examine the effect of long-term storage on biodiesel's properties. A major concern regarding the large-scale commercial use of biodiesels is their oxidation stability [9,20,21]. As discussed in these studies, the unsaturated fatty acids present in biodiesels are susceptible to oxidation, leading to the formation of peroxides and hydroperoxides, and subsequently aldehydes and ketones, and finally resins. The long-term storage and improper handling can also lead to excessive moisture uptake and increase in the total acid value, making biodiesels unsuitable for use in engines. In order to evaluate the long-term storage effect and the practicality of remediating deteriorated fuels, the biodiesels which were originally produced and received from IIT-Kanpur in 2012 were evaluated after almost 2 yr of storage. They were subsequently retransesterified at the Illinois Sustainability Technology Center (ISTC) in Champaign, IL. Test procedure and conditions for retransesterification are briefly described in Secs. 2 and 3.

Properties of the 2012-biodiesels and 2014-biodiesels (after retransesterification) were compared to evaluate the extant of degradation and the ability to bring deteriorated fuels back into specification. After retransesterification, the total glycerol of both J100 and K100 biodiesels were brought within ASTM 6751 specification, as indicated in Table 1. The biodiesel yields for the second transesterification were 83.01% (5.72 l of neat fuel made from 6.89 l of degraded fuel) for Jatropha and 70.51% (5.8–8.24 l) for Karanja. Total glycerol was the primary concern that led to the

Table 1 Free and total glycerol content of J100 and K100 before and after retransesterification

	Jatropha (J100)		Karanja (K100)		
Fuel	Before	After	Before	After	ASTM standard
Free glycerol	0.004	0.005	0.0023	0.012	0.020 mass % max
Total glycerol	1.040	0.032	0.295	0.063	0.240 mass % max

Table 2 Fatty acid profiles for J100 and K100 before and after retransesterification. Values are in percent.

Fatty acid (C *aa*:*b*)[a]	J100 before	J100 after	K100 before	K100 after
Myristic acid methyl ester (C 14:0)	—	—	—	—
Palmitic acid methyl ester (C 16:0)	14.1	15.8	8.6	9.5
Palmitoleic acid methyl ester (C 16:1 (9 c))	—	0.7	—	0.1
Stearic acid methyl ester (C18:0)	7.0	7.4	6.6	6.5
Oleic acid methyl ester (C18:1 (9C))	37.9	41.5	55.2	58.2
Oleic acid methyl ester (C18:1 (11C))	1.0	0.2	0.5	0.3
cis-9-*cis*-12-Octadecadienoic acid methyl ester (C18:2 9C, 12C)	38.4	33.5	16.6	14.9
cis-9-*cis*-12-*cis*-15-Octadecatrienoic acid methyl ester (C18:1(9C, 12C, 15C))	—	—	—	1.5
Arachidic acid methyl ester (C 20:0)	—	0.4	2.2	1.5
Cis-11-Eicosenoic acid methyl ester 20:1 11C	—	—	—	1.2
Behenic acid methyl ester (C 22:0)	—	0.2	4.9	4.5
Lignoceric acid methyl ester(C 24:0)	—	—	1.5	1.2
Other	1.6	0.3	3.9	0.6

[a]*aa* and *b* denote the number of carbons and number of double bonds, respectively, in fatty acid chain.

Table 3 Physicochemical properties of diesel: J100, J30, K100, and K30

Fuel property	Test method	Diesel	J100	J30	K100	K30	ASTM-D6751 08a
Acid value (mg KOH/g)	AOCS Cd3d-63	—	2.11	0.73	4.29	1.39	0.5 max
Carbon content (wt.%)	GC–MS (HP-6890)	86.80	76.22	83.51	76.83	83.69	—
Hydrogen content (wt.%)	GC–MS (HP-6890)	12.97	12.49	12.85	11.83	12.66	—
Oxygen content (wt.%)	GC–MS (HP-6890)	0.23	11.29	3.63	11.34	3.647	—
Cetane number	ASTM D5291	41.2	84.99	60.32	66.14	55.27	
Cloud point (°C)	Phase Technology	−11	4.3, 4.4	−8.5, −8.8	17.3, 18.2	1.0, 1.8	Report to customer
Copper corrosion	ASTM D130	—	1A	1A	4A	4A	3A
Density at 15 °C (kg/m3)	ASTM D445	849.20	888.80	864.70	899.60	866.56	—
Flash point (°C)	ASTM D93	69.44	170.6	77.2	143.3	76.1	93.0°Cmin.
Heat of combustion (kJ/kg)	ASTM D240	45,460.0	38,094.0	43,250.2	37,737.0	43143.1	—
Lubricity (HFRR, μm)	ASTM D6890	0.599	192.27	383.43	185.22	438.396	520 max
Oxidative stability (110 °C, hr)	EN 14112	—	0.04	0.02	0.04	0.02	0.05
Sulfur content (ppm)	OES Spectrometer	11	8.74	8.86	9.43	Not available	15 (ppm) max
Viscosity at 40 °C (cSt)	ASTM D445	2.50	5.15	3.41	5.70	3.40	1.9–6.0
Vapor pressure (pa)	ASTM D5191	1000	<1.0	3.02	<1.0	<1.0	

reprocessing, but there were other properties that degraded as a result of the long-term storage, as discussed in Sec. 2.

2 Biodiesel Properties

All measured properties of the test fuels are given in Tables 1–3. Table 2 shows the fatty acid profiles of J100 and K100 biodiesels received in 2012 and after reprocessing in 2014. Fatty acid profiles were determined using the gas chromatography–mass spectroscopy (GC–MS) (Agilent, HP 6890) system. Fatty acid composition of biodiesel plays a key role in its physical and chemical properties as well as its engine performance. The composition of biodiesel, mainly carbon chain length and degree of unsaturation, has a significant effect on cetane number, cold flow properties, and oxidation stability. Properties reported before and after processing indicate some degradation of both methyl esters. As shown in Table 2, major constituents of J100 and K100 include the unsaturated components, namely, oleic acid (41.7%, 58.5%) and octadecadienoic acid (33.5%, 16.4%), and unsaturated components, namely, palmitic acid (16.5%, 9.6%) and stearic acid (7.4%, 6.5%). These numbers indicate that both J100 and K100 have high degree of unsaturation (i.e., presence of double bonds), and thus relatively high cetane numbers [21] and susceptibility to oxidation. As noted earlier, oxidative degradation leads to the formation of peroxides and hydroperoxides, which are known cetane number enhancers [22].

Table 3 lists the physical–chemical properties of the five fuels used in the present study. As indicated, compared to the conventional diesel, J100 and K100 have higher density, significantly higher viscosity, and much lower vapor pressure. These properties, especially viscosity and vapor pressure strongly influence the fuel injection, atomization, and vaporization characteristics. These aspects were, however, not investigated in the present study. Other notable properties include the caloric value, which affects the engine combustion and performance characteristics (power output, HRR, BSFC, BTE, etc.), and cetane number, which determines the autoignition behavior. As indicated in Table 3, the caloric values (lower heating values) of J100 and K100 were ∼16% and 17% lower, while the cetane numbers were noticeably higher compared to diesel. The higher cetane numbers can be attributed to relatively higher degree of unsaturation and presence of cetane enhancers, such as peroxides and hydroperoxides, formed due to the long storage period of biodiesels.

3 Experimental Setup and Procedure

Retransesterification was carried out with dry methanol and sodium hydroxide as a catalyst. Catalyst quantity and reaction conditions were estimated from small scale tests of Jatropha and Karanja and large scale testing of refined corn oil. Temperature was kept at 85 °C. Small scale tests using 100 g refined corn oil are known to have full conversion with the addition of 0.75% m sodium hydroxide and 29.3% m methanol (1 mol oil:8 mol methanol) relative to the whole oil mass and heating at 85 °C for 1 hr of reflux with stirring. The temperature of 85 °C was selected so that we would be at reflux temperature for the methanol for added mixing. Tests reactions were run in relation to the glyceride content of the oils. If we assumed all of the oil was triglycerides, which was equivalent to 72× the glyceride content. Reactions were run adding catalyst and methanol in varying multiplication factors, 7×, 14×, and 21×, of the glyceride content of the oil. These tests indicated that the conditions were sufficient for the reclamation of aged Jatropha but the reaction needed be repeated a second time for the full conversion of the aged Karanja sample.

Large scale tests for refined corn oil are known to take 2.5 hrs in the 5 gal reactor compared to 1 hr reaction time in the small scale tests. It was presumed that the Jatropha and Karanja samples would also require additional reaction time when run at the larger scale. Samples were collected at 3 hrs, 4.5 hrs, and 6 hrs time intervals to test the FAME by GC–MS for the completeness of the reaction. It was found that after 6 hrs the glyceride content was still beyond ASTM limits and the reaction was repeated with samples collected at the same time intervals for testing by GC–MS.

Experiments were performed in a single cylinder, four-stroke, CI (Caterpillar 34010) engine using five fuels, namely, J100, K100, J30, K30, and conventional diesel, at three different SOIs: −5 deg, −1 deg, and 3 deg ATDC. This resulted in 15 different experimental conditions. Other operating conditions are provided

Table 4 Engine specifications and test conditions

Description	Type
Engine model	Caterpillar 3401E
Bore	137.2 mm
Stroke	165.1 mm
Displacement	2.44 L
Compression ratio	16.3:1 (measured on modified cylinder head)
Engine speed	1500 rpm
Fuel quantity per injection	100 mm^3
Injection pressure	1584 bar
Combustion air system	Simulated turbocharger with air-to-air after cooler[a] 0.6 bar intake manifold pressure 0.4 bar exhaust backpressure 40 °C intake manifold temperature
Fuel injection system	HEUI 315B, six-hole tip
Injector hole size	169 μm (mini-sac), 126 deg Angle

[a]An external air compressor was used to supply the combustion air at the conditions shown.

in Table 4. Note that a fixed fuel volume was used in all the tests. As a consequence, the mass flow rates for biodiesels were higher compared to that diesel. The measured average mass flow rates were 3.55 kg/hr, 3.65 kg/hr, and 3.8 kg/hr for the diesel, J100, and K100, respectively. The injection system employs a Caterpillar hydraulically actuated, electronically controlled unit injector (HEUI) mini-sac with six holes. Details of the injector nozzle geometry can be found in Fig. 2 of Ref. [23]. The HEUI system uses hydraulic pressure from the oil to raise the fuel pressure to the desired level for direct injection. This is achieved by an internal differential piston, which multiplies the oil rail pressure to a high fuel injection pressure. This injector uses a pressure intensification ratio of approximately 6.6 between the oil rail pressure and injection pressure [24]. Parameters such as the injection timing, duration, and quantity are controlled by a solenoid that is connected to the engine's electronic control unit. The rate of injection profile was measured using a Bosch-Type rate meter [23].

A mass flow meter (Sierra Instruments, 780S) was used to measure the engine combustion air mass flow rate. This instrument has a hot wire anemometer calibrated for air and programed to provide a mass flow rate measurement. The fuel flow rate was measured by a fuel balance system incorporated into a specially designed fueling cart for low fuel volume experiments and facilitated switching of fuels. Fuel flow data were logged into a data logging system at a frequency of 1 Hz. Further details regarding the test cell setup can be found in previous work [25]. A piezoelectric, water-cooled pressure transducer with a charge amplifier was used to acquire the cylinder pressure data. The cylinder pressure and crankshaft angle encoder signals were measured using a commercial indicating system and software for data processing [26]. Parameters such as intake/exhaust air pressures and temperatures, engine coolant temperature, engine oil temperature, and others were controlled using closed-loop proportional-integral-derivative control through a system that was also used for logging data. Gaseous emissions were measured by using a chemiluminescent analyzer for volumetric measurements of NOx, an infrared analyzer for CO and CO_2, and a paramagnetic detector for O_2 measurements.

Visualization of in-cylinder combustion events was performed by using AVL VisioScope™ optical system, in which image processing was done using AVL's Thermo Vision™ software. The optical system consists of a 4-mm diameter endoscope and a 640×480 pixel, VGA color digital camera with 12-bit resolution. The two-color optical pyrometry was used to postprocess pixel resolved soot temperature and soot volume fraction (SVF) [27]. As shown in Fig. 1, the engine cylinder head was modified in order to accommodate cylinder pressure transducer and the endoscope. The endoscope and pressure transducer access was gained by machining through the cylinder head casting and breaking through the cylinder head between intake and exhaust valves. This arrangement minimizes the effects of the squish area between the piston crown and the cylinder head at top dead center. The

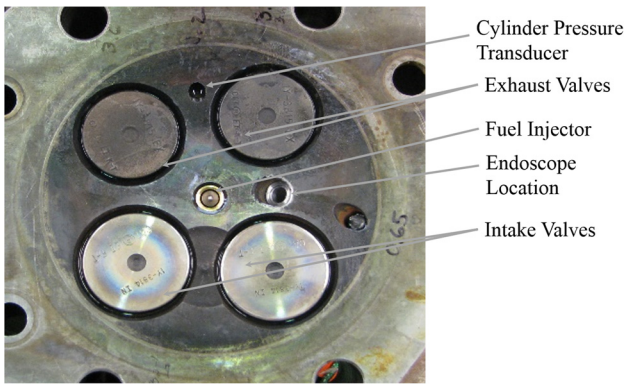

Fig. 1 Cylinder head modification

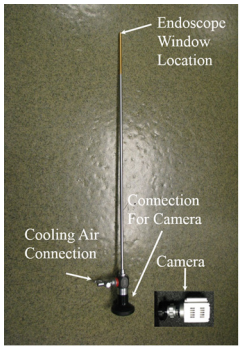

(*a*)

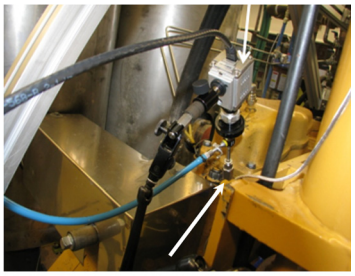

Arrow showing camera connected to 4mm endoscope entering into combustion chamber

(*b*)

Fig. 2 Endoscope experimental setup on engine (*a*) endoscope and (*b*) mounted assembly on engine head

endoscope data was recorded in CA resolved time domain, where all snapshots were taken at 0.5 deg CA interval. To ensure maximum observation, a 60 deg endoscopic window was used to acquire images. The camera's frame rate was 50 fps with 10 μs exposure time that corresponds to 0.09 deg for the engine running at 1500 rpm. Figure 2 shows the location of endoscope access and a sample view of the combustion. More details regarding the endoscope system used can be found in Ref. [27].

4 Results and Discussion

4.1 Engine Combustion and Performance Data. Figure 3 presents the variation of cylinder pressure and HRR with respect to CA at three different SOIs for diesel, J100 and K100. For all three SOIs, results indicate shorter ignition delays (approximately 1.5 deg CA) with two biodiesels (J100 and K100) compared to baseline diesel due the higher cetane numbers of biodiesel. Note that as a result of higher viscosity, the physical delay related to the fuel injection process is increased for the two biodiesels. This has the effect of increasing the ignition delay for biodiesels. However, this increase is expected to be small compared to the decrease in chemical ignition delay due to the significantly higher cetane numbers of these biodiesels. As a consequence of longer ignition delay for diesel, there is increased fuel–air mixing, and therefore more fuel mass is burned during premixed combustion phase for diesel, as indicated by the rate of heat release (ROHR) plots in Fig. 3. Increased premixed combustion may also be partly attributed to finer fuel atomization as a result of increased cavitation in the injector nozzles in case of diesel due to its relatively higher vapor pressure [28]. The HRR plots further indicate that while the premixed heat release is higher for diesel, the amount of diffusion heat release is nearly the same for all three fuels, except that the HRR during diffusion combustion is higher for diesel due to its higher heating value. The corresponding results for the two blends (J30 and K30) shown in Fig. 4 exhibit similar trends, except that the differences between the diesel and biodiesel blends (J30, and K30) are reduced compared to those for pure biodiesels (J100 and K100), as expected. It is also interesting to note that there are no significant differences between the two biodiesels in terms of their ignition and combustion characteristics. Regarding the effect of SOI, the pressure and HRR plots indicate that the ignition delay decreases as the SOI is delayed from −5 deg to −1 deg ATDC, since the cylinder pressure is higher during ignition for the latter case. However, as the SOI is further delayed from −1 deg to 3 deg ATDC, ignition occurs at lower pressure during the expansion stroke, and the ignition delay increases. Consequently, the relative amount of premixed burn is higher for the 3 deg ATDC SOI case, as indicated by the HRR plot.

Ignition delays can also be determined based on the consideration that the start of combustion (SOC) corresponds to the peak value of the second derivative of pressure, and it coincides with

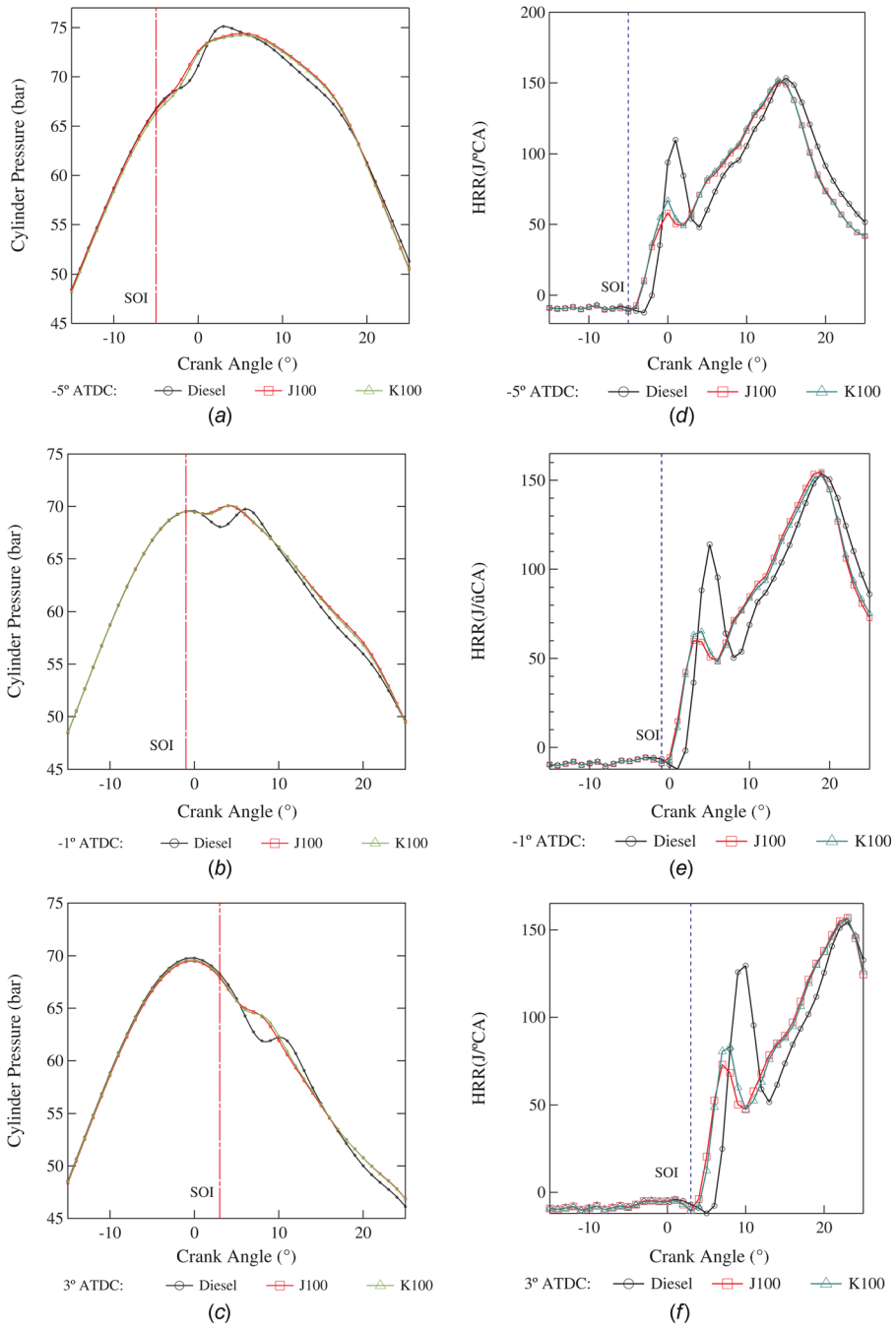

Fig. 3 Cylinder pressure and HRR for diesel: J100 and K100 at three different SOIs. Vertical line indicates the SOI value.

the occurrence of ignition. This methodology is generally more robust than using the first derivative to determine SOC due to the fact that first derivative varies significantly with load and speed [29]. Table 5 provides SOCs and ignition delays for all test cases, based on the peak value of the second derivative of pressure. These results are generally consistent with the ignition delays determined from pressure and HRR plots presented in Figs. 3 and 4. Finally, the ignition delay can also be determined from the measured percentage mass burn fraction (MBF) data of fuels. These results based on MBF_{10} (not shown) were also consistent with the pressure and HRR plots discussed above. In addition, the MBF data indicated somewhat earlier combustion phasing and shorter combustion duration for biodiesels and their blends compared to diesel. This may be due to shorter ignition delay and higher oxygen content in biodiesel, which could lead to relatively earlier completion of combustion.

The effect of using biodiesels on engine performance is characterized in terms of the measured IMEP, BTE, and BSFC. Figure 5 plots the IMEP versus SOI for various fuels. The IMEP values are lower for the biodiesels and their blends compared to conventional diesel. This can be attributed to the higher heating value and the longer ignition delay for diesel, with the latter resulting in increased fuel-burn during the premixed combustion phase and thus greater pressure rise for diesel. In addition, results indicate that the IMEP decreases as the SOI is retarded. This is due to the fact that combustion occurs during the expansion stroke for the late injection cases. Note that all data plotted here are averaged values taken over at least four tests under the same conditions.

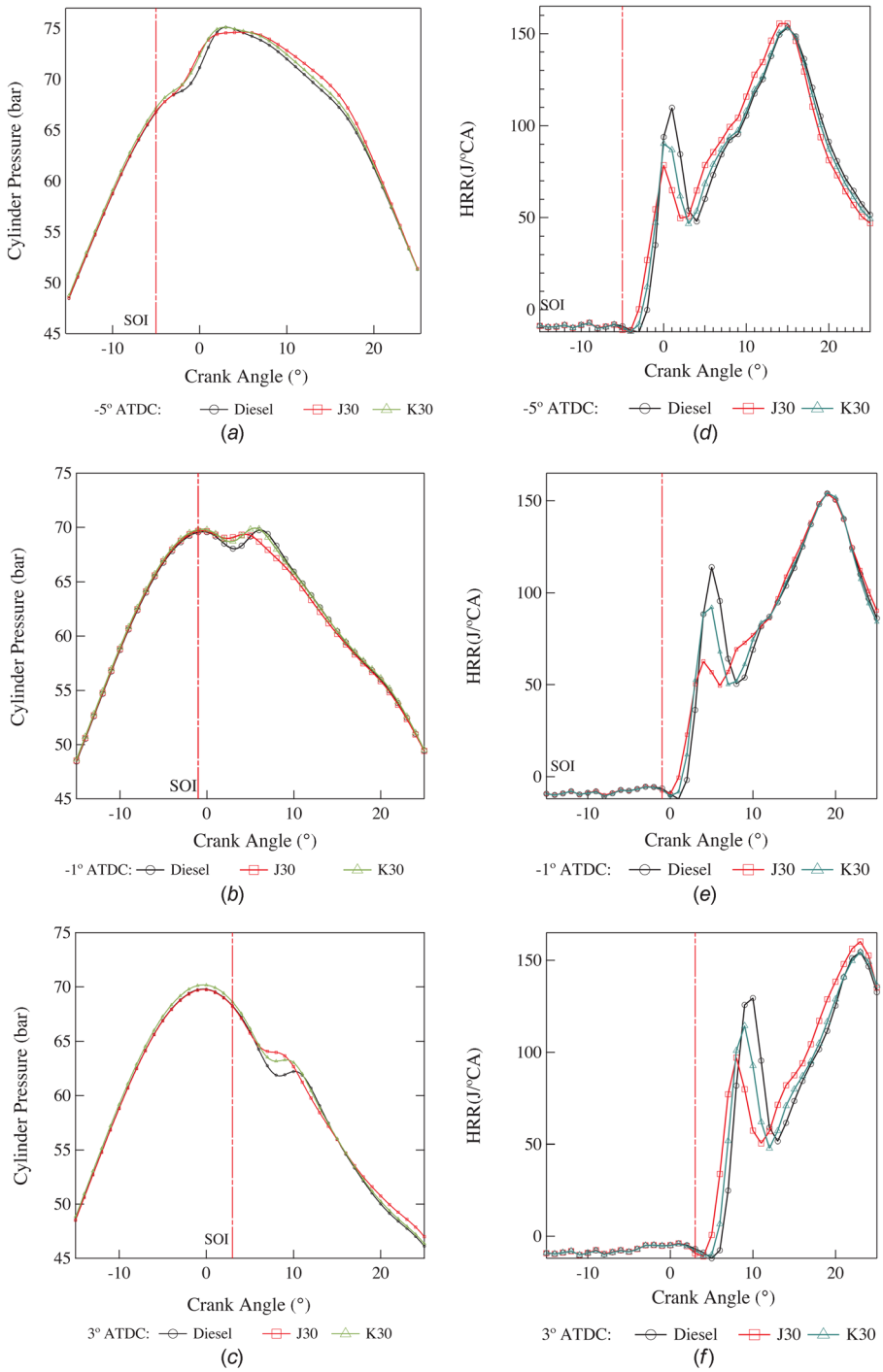

Fig. 4 Cylinder pressure and HRR for diesel: J30 and K30 at three different SOIs. Vertical line indicates the SOI value.

Error bars show standard deviations for the data. As indicated in Fig. 5, standard deviation decreases as the SOI is retarded, implying smaller fluctuations, which may be attributed to more complete combustion in conjunction with timely exhaust of the emission gases.

Figure 6 presents the variation of BTE with respect to SOIs for different fuels. The BTE values are higher for biodiesel (K100 and J100) and their blends (K30 and J30) compared to baseline diesel at all injection timings. This can be attributed to the oxygenated nature of biodiesels, resulting in more complete combustion and increased thermal efficiency. In addition, the BTE improvement may be due to both the advanced ignition timing as a result of reduced ignition delay and the lower heat loss since the combustion temperatures would be lower with less energy input for combustion. These results are also consistent with those reported by Agarwal et al., who observed higher BTE for Karanja biodiesel [17]. Furthermore, results indicate that for all test fuels, BTE increased as the injection timing was advanced. As discussed by Agarwal et al. [30], with advanced SOI, a larger amount of evaporated fuel accumulates in the combustion chamber during the ignition delay period, and burns more rapidly in the premixed combustion phase, therefore causing rapid increase in pressure. Consequently, the power output and BTE increase with relatively earlier injection.

Table 5 Start of combustion (SOC), based on second derivative of cylinder pressure, and ignition delay time for diesel: J30, K30, J100, and K100

SOI	Fuel type	SOC (deg CA)	Ignition delay time in terms of CA degrees
−5 deg ATDC	Diesel	3.5	8.5
	J30	2.3	7.3
	K30	2.9	7.9
	J100	1.6	6.6
	K100	1.9	6.9
−1 deg ATDC	Diesel	7.6	8.6
	J30	6.2	7.2
	K30	7.1	8.1
	J100	5.8	6.9
	K100	5.9	6.8
3 deg ATDC	Diesel	12.3	9.3
	J30	10.6	7.6
	K30	11.6	8.6
	J100	9.8	6.8
	K100	10.1	7.1

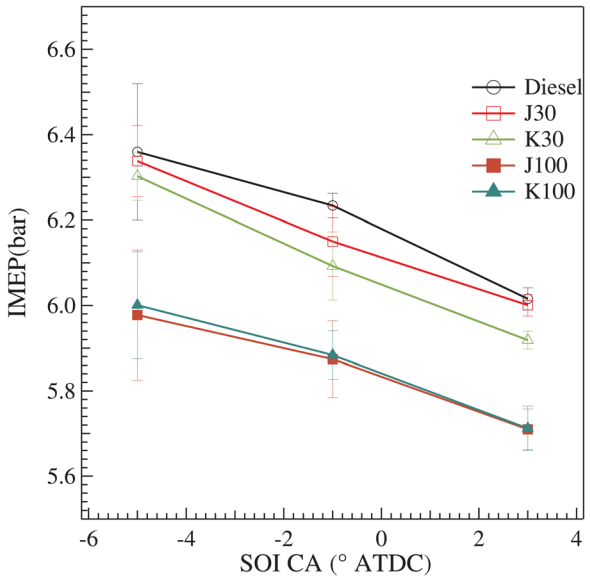

Fig. 5 IMEP plotted versus SOIs and diesel: J30, K30, J100, and K100

Figure 7 shows the variation of BSFC with SOIs for different fuels. The BSFC for biodiesels and their blends is higher compared to that for diesel, and this can be attributed to lower heating value of biodiesel, since the engine needs to consume additional biodiesel to provide the same power output as that from diesel. Thus, the lower power output and higher BSFC for biodiesels are related to their lower heating values. It is also interesting to note that both BTE and BSFC are higher for biodiesels, implying that the improvement in efficiency is not fully compensated by the loss of power output with the use of biodiesel. These results are in agreement with the experimental data reported by Agarwal et al. [31]. Regarding the effect of SOI, results in Fig. 7 further indicate that for all fuels, an early injection results in to lower BSFC, which is due to the higher engine power with early injection, as noted earlier.

4.2 Emission Characteristics. Emission data is reported in terms of mass emissions of CO (BSCO), unburned HC (BSHC), and NOx (BSNOx). Figure 8 presents the BSCO emissions versus

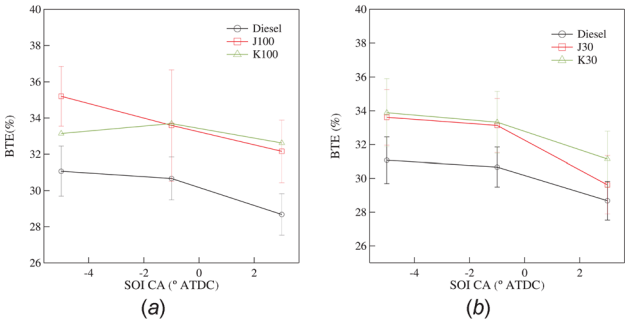

Fig. 6 BTE versus SOIs for diesel: J1000 and K100 (*a*) and J30 and K30 (*b*)

SOIs for diesel, J100, K100, J30, and K30. The corresponding data for BSHC is shown in Fig. 9. As indicated, CO and HC emissions are generally reduced with biodiesels and their blends compared to conventional diesel. This can be attributed to the oxygenated nature of biodiesels, which promotes more complete combustion, and thus oxidation of CO to CO_2 and reduction of HC in the exhaust. These results are in agreement with those reported by other researchers [7,13] dealing with oxygenated fuels including Jatropha and Karanja biodiesels. In addition, Figs. 8 and 9 indicate that for all the five fuels, CO and HC emissions are higher with late injection. This may be attributed to the fact that with late injection, the ignition and combustion processes occur during the expansion stroke, lowering the combustion duration and leading to incomplete combustion.

Figure 10 plots the variation of tailpipe BSNOx with SOIs for different fuels. These results are consistent with several previous studies [1,2,7,13,15], which reported increased NOx emissions with biodiesels compared to conventional diesel. NOx formation in diesel engine depends on a number of factors, including the peak temperature of the burned gas, residence time available for combustion and NOx formation reactions to occur, fuel's molecular structure, as well as oxygen content. Regarding the fuel molecular structure, previous studies [32–37] using various combustion systems, including engine, shock tube, and flames, have attributed increased NOx associated with biodiesels to the degree of unsaturation, i.e., the number of double/ triple bonds as well as the fatty acid chain length. As indicated in Table 1, both biodiesels (J100 and K100) contain significant amounts of long-chain fatty acid methyl esters with one or two double bonds. Thus, increased NOx may partly be due to relatively higher degree of unsaturation in Jatropha and Karanja biodiesels. Ban-Weiss et al. [40] reported that unsaturated molecules have higher adiabatic temperature than saturated molecules resulting in higher flame temperature with biodiesels in comparison to baseline diesel. Higher NOx emissions with biodiesels could also partly be due to higher cetane number of these two biodiesels, resulting in shorter ignition delays, as noted earlier, and availability of thus longer reaction times for NOx formation. In addition, the reduced soot formation with biodiesel (discussed in Sec. 4.3) may lead to higher flame temperatures due to the lower radiative heat losses (from soot), but resulting in increased thermal NOx from biodiesel. Results in Fig. 9 further indicate that for all test fuels, since the SOI is delayed, it leads to reduction in NOx emission. This may be attributed to lower flame temperatures and reduced residence time for NOx formation with late injection.

4.3 Endoscopic Data Analysis. Figure 11(*a*) presents in-cylinder 2D images depicting the spray and combustion processes for diesel, J30 and J100 for the case with SOI = −5 deg ATDC. These images were then processed using the optical pyrometry technique to extract soot radiation temperatures and SVF for each radiating pixel. The soot radiation temperature is

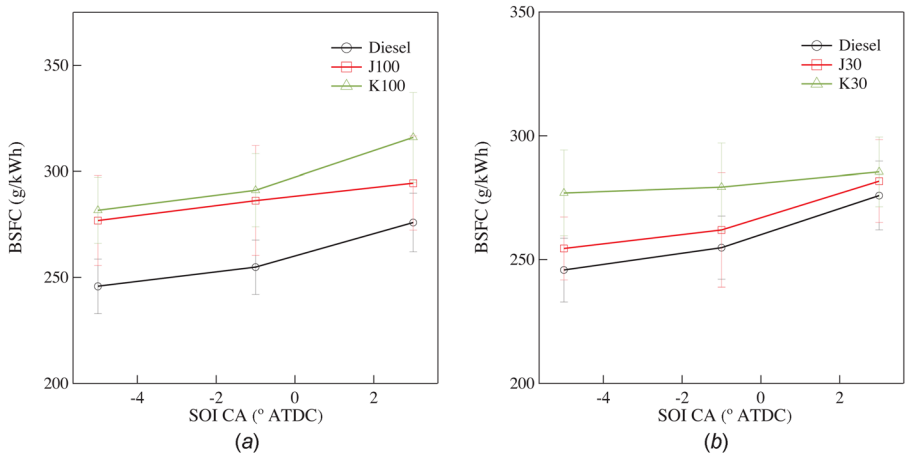

Fig. 7 BSFC versus SOIs for diesel: J100 and K100 (*a*) and J30 and K30 (*b*)

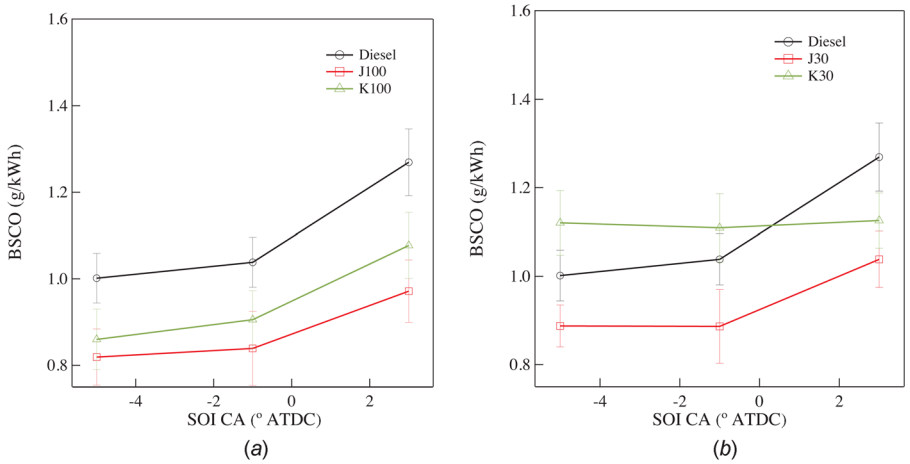

Fig. 8 BSCO versus SOI for diesel: J100 and K100 (*a*) and J30 and K30 (*b*)

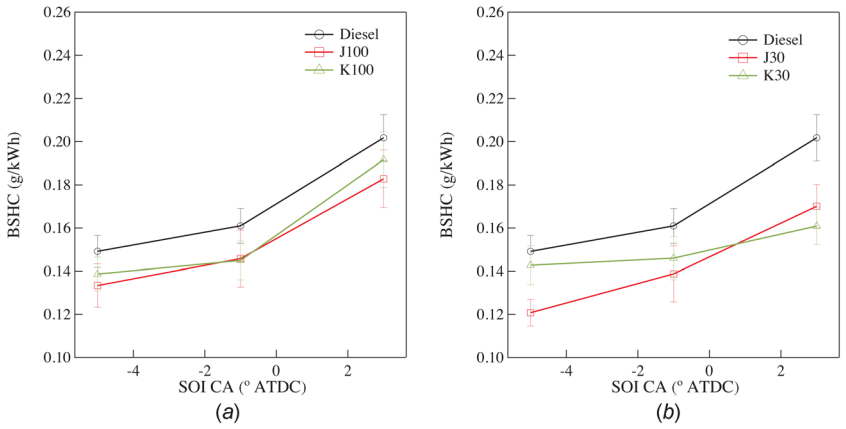

Fig. 9 BSHC versus SOI for diesel: J100 and K100 (*a*) and J30 and K30 (*b*)

determined by the ratio of light intensities at specific wavelengths. Details are provided in Refs. [27,38]. Thermal video images to obtain temperature distribution in flames have also been reported by Desmira et al. [39]. As discussed in Ref. [27], the wavelengths used for this study were 470 nm, 540 nm, and 625 nm. The ratios of light intensities at these three wavelengths determine the soot temperatures ranging between 1800 K and 3000 K. Pixels below 1800 K do not appear in the image and above 3000 K are considered as erroneous. The pixels above 3000 K are displayed in white and are not used for average temperature or SVF. A similar

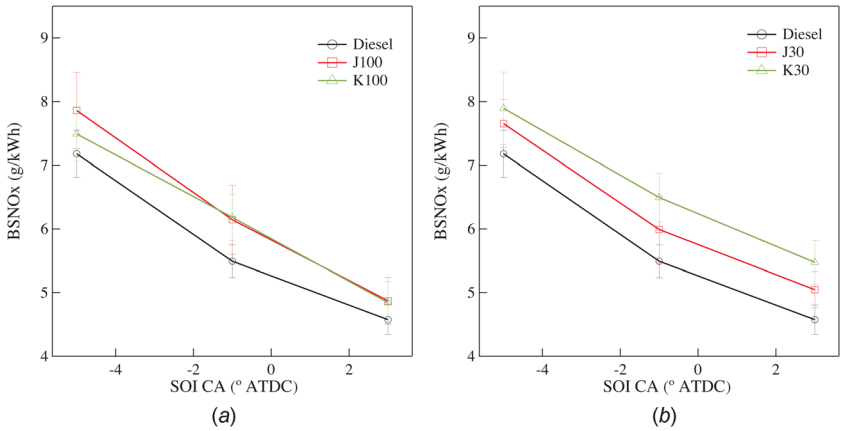

Fig.10 BSNOx versus SOI for diesel: J100 and K100 (*a*) and J30 and K30 (*b*)

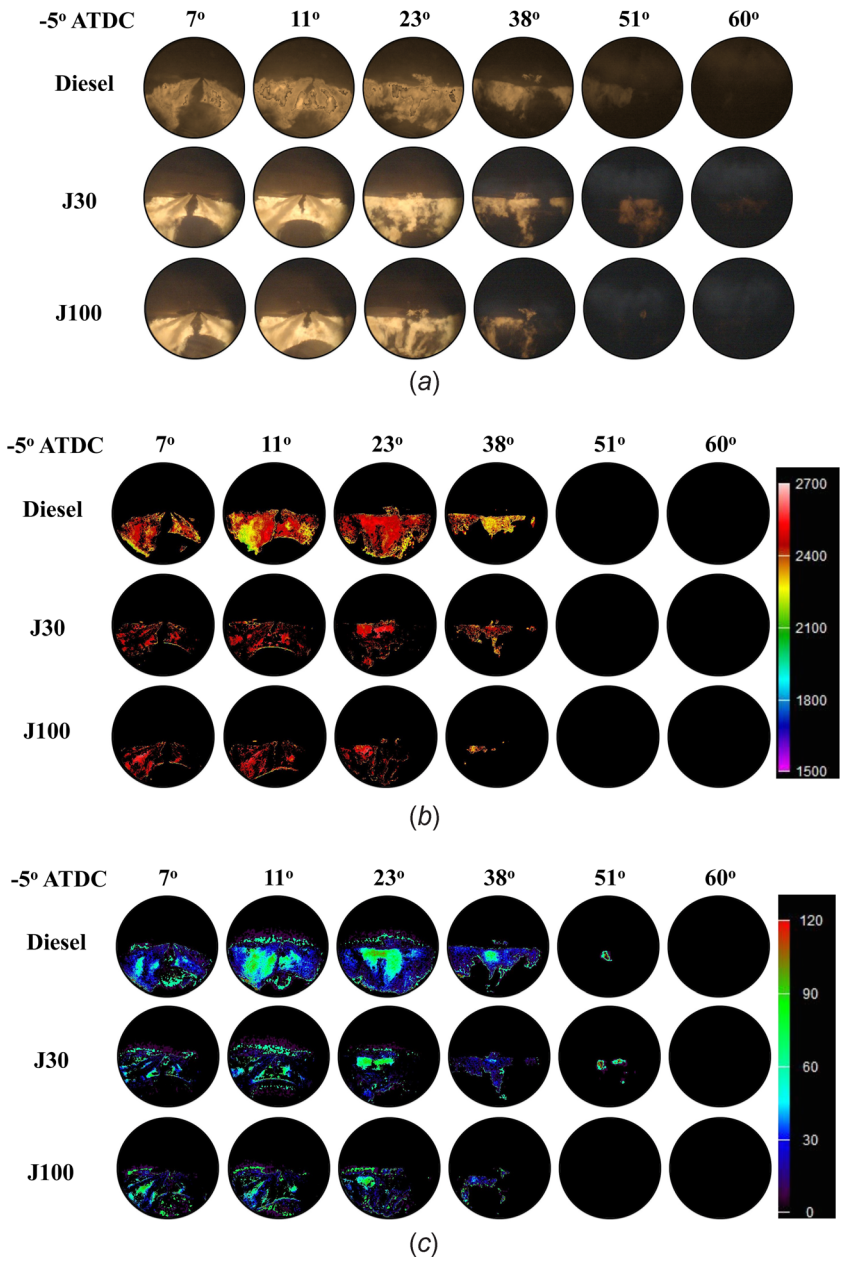

Fig. 11 Two-dimensional images at different CAs for diesel, J30 and J100, depicting the combustion process (*a*), soot radiation temperature (*b*), and SVF distribution, (*c*) SOI = −5 deg ATDC

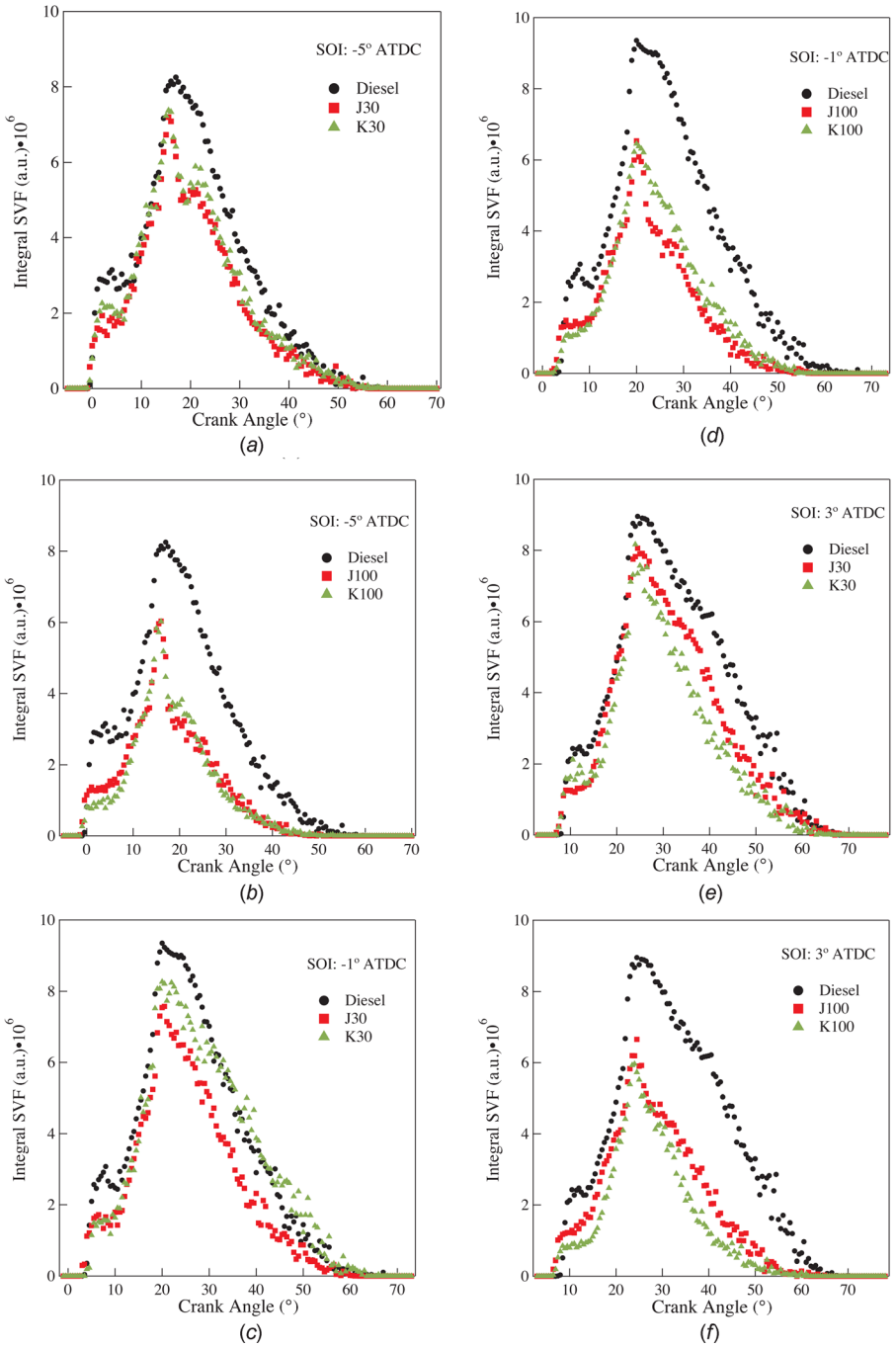

Fig. 12 Integrated SVF versus CA for diesel: J30 and K30 (*a*)–(*c*) and J100 and K100 (*d*)–(*f*) for the three SOIs

approach was used to calculate the SVF. However, as discussed in Ref. [27], soot measurement requires the absolute light intensity at each wavelength, in contrast to the relative light intensities used in the temperature calculation. Figures 11(*b*) and 11(*c*) show, respectively, the 2D temperature and SVF distributions at different CAs, calculated from the corresponding images in Fig. 11(*a*). A more complete set of images for various cases are provided in Ref. [38]. Qualitatively, the images in Figs. 11(*b*) and 11(*c*) for the three fuels indicate that both the soot radiation temperature and SVF are noticeably reduced with biodiesels compared to baseline diesel. An important implication from these results, albeit qualitative, is that soot production is significantly reduced using biodiesels.

While the images in Figs. 11(*b*) and 11(*c*) are presented at different CAs, the temporal trends can be more easily discerned by computing the integral values and plotting them with respect to CA. Figure 12 presents the integral SVF versus CA for the five test fuels and different SOIs, while Fig. 13 presents the average soot radiation temperature versus CA for the same cases. As discussed in Ref. [27], the integral values shown in Fig. 12 are based upon the KL (product of soot absorption coefficients (K) and optical length) value determined from two-color optical pyrometry. For these images, the KL value of each pixel, which varies between 0.0 and 3.0, was summed and recorded as an integral value. Therefore, the overall integral value is dependent upon the average KL factor of each pixel and the total number of radiating pixels.

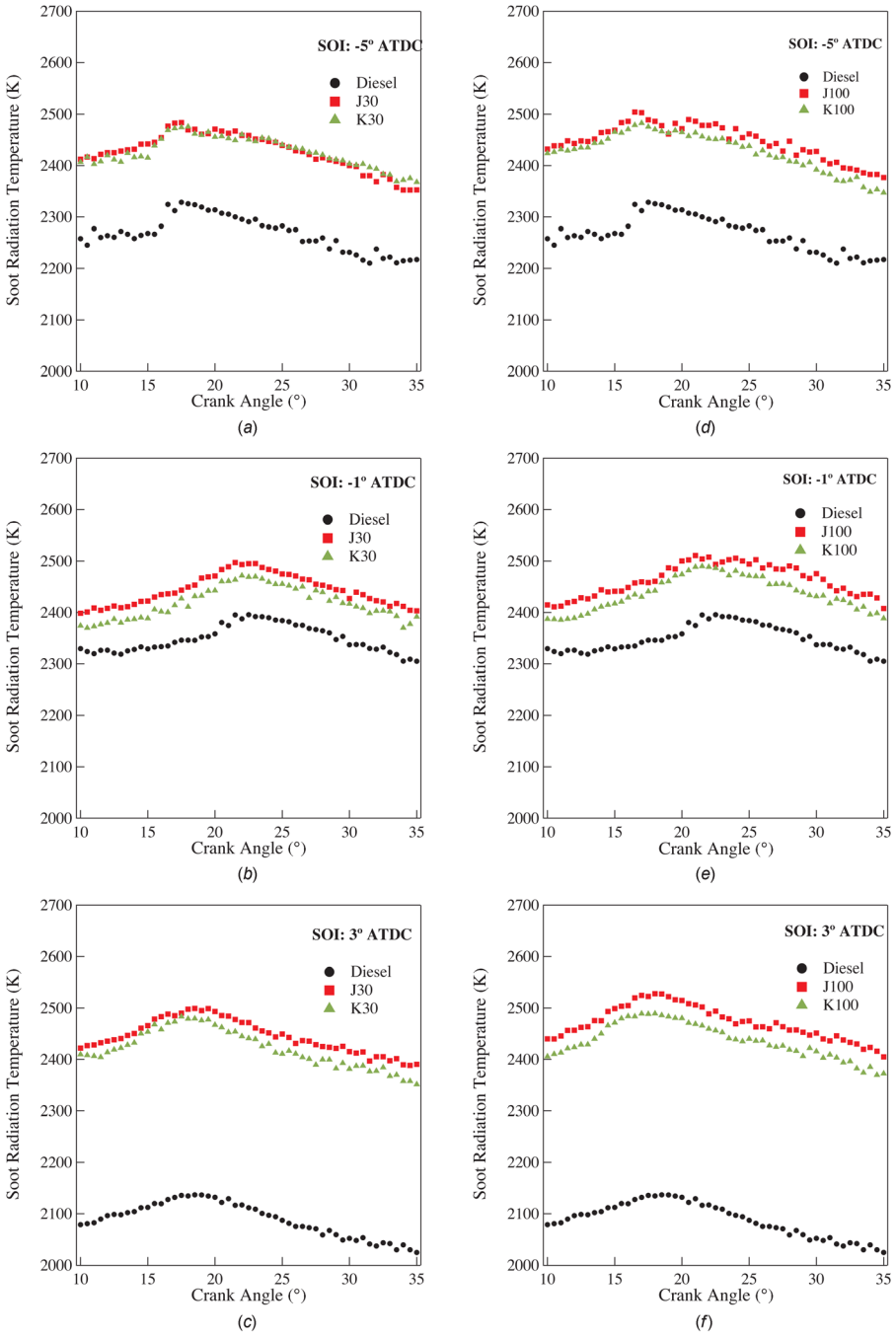

Fig. 13 Soot radiation temperature versus CA for diesel: J30 and K30 (*a*)–(*c*) and J100 and K100 (*d*)–(*f*)

An important observation from Fig. 12 is that SVF values are significantly reduced with biodiesel and their blends compared to baseline diesel. This can be attributed to two factors, i.e., the absence of aromatic compounds in biodiesels and the oxygenated nature of biodiesel, which reduced the amount of soot formed in the fuel-rich regions. Results further indicate that for all fuels, the peak SVF values first increased as SOI was retarded from −5 deg to −1 deg, and then decreased slightly as SOI was further retarded from −1 deg to −3 deg ATDC. This variation was due to the effect of SOI on ignition delay and heat release during premixed combustion. In addition, the CAs corresponding to the peak SVF values are the same for all the five fuels, and correspond to the end of fuel injection. The subsequent decrease in SVF indicates the dominance of soot oxidation process for all the five fuels. Figure 13 shows the average soot radiation temperature versus CA for the same cases as discussed in the context of Fig. 12. The temperatures are noticeably higher for biodiesel and their blends compared to baseline diesel. This correlates well with higher SVFs (Fig. 12) resulting in higher radiation heat loss for diesel compared to biodiesel. Higher in-cylinder peak temperatures for biodiesel further support the observation regarding higher NOx emissions for these fuels, as discussed earlier.

4 Conclusions

Engine performance and emission characteristics have been investigated using conventional diesel, Jatropha and Karanja methyl esters (J100 and K100), and their blends with diesel (J30

and K30). The effect of long-term storage on the biodiesel oxidative stability was also examined. The biodiesels produced at IIT Kanpur, India, were tested in a single cylinder, four-stroke, compression ignition engine at ANL, USA, and the effects of various fuels at different SOIs (−5 deg, −1 deg, and 3 deg ATDC) were characterized. In addition, an endoscopy system was employed to visualize combustion events and examine the in-cylinder temperature and soot distribution during combustion. Important observations are:

(1) The long-term storage of biodiesel leads to increase in glycerol content, acid value, and cetane number for these two biodiesels, indicating some oxidation of unsaturated fatty acids. With retransestrification, the free and total glycerol levels can be reduced to meet the ASTM 6751 standards.
(2) The ignition delays were longer for diesel compared to biodiesels. This leads to increased fuel–air mixing and higher pressure and HRRs during the premixed combustion phase for diesel. While the shorter ignition delays with biodiesels may primarily be attributed to their relatively higher cetane numbers, higher viscosity and lower vapor pressure of biodiesel may also play a role, as these properties significantly affect the fuel atomization and vaporization characteristics.
(3) IMEP is found to be lower for biodiesel compared to baseline diesel, which may be due to the higher calorific value (LHV) and longer ignition delay of baseline diesel. In contrast, both the BTE and BSFC were higher for biodiesels compared to diesel, with the implication that improvement in combustion efficiency due to the oxygen content of biodiesels is not fully compensated by the loss of power output due to their relatively lower heating value. In addition, the BTE improvement with biodiesel may be due to both the advanced ignition timing as a result of reduced ignition delay and the lower heat loss since the combustion temperatures are lower with less energy input for combustion.
(4) CO and HC emissions are lower with biodiesels compared to those with diesel. This can be attributed to the oxygenated nature of biodiesels, which promotes more complete combustion. However, NOx emissions (BSNOx) were higher with biodiesels, which may be due to several factors, such as higher temperatures, longer residence time, and higher level of unsaturation due to the presence of long-chain fatty acid components with double bonds in biodiesels. Analysis of the in-cylinder images of combustion events indicate considerably lower SVF and higher soot radiation temperatures for biodiesels compared to diesel. This may be due to the absence of aromatic compounds in biodiesels and their oxygenated nature.
(5) For all test fuels, IMEP decreases as SOI is retarded, since combustion occurs during the expansion stroke for the late injection cases. The late injection also results in lower BTE, higher BSFC, and increased CO and HC emissions, but lower NOx emissions due to lower peak in-cylinder temperatures.

Acknowledgment

The assistance and many insights provided by Dr. B. K. Sharma at the Illinois Sustainability Technology Center (ISTC) at Urbana-Champaign in performing the biodiesel characterization and throughout this research are greatly appreciated. We also acknowledge the assistance of Dr. Stephen Ciatti, Dr. Anita Ramirez, and Mr. Timothy Rutter for conducting the experiments.

This manuscript has been created in collaboration with UChicago Argonne, LLC, operator of ANL (Argonne). Argonne, a U.S. Department of Energy Office of Science laboratory, is operated under Contract No. DE-AC02-06CH11357. The U.S. Government retains for itself, and others acting on its behalf, a paid-up, nonexclusive, irrevocable worldwide license in said article to reproduce, prepare derivative works, distribute copies to the public, and perform publicly and display publicly, by or on behalf of the Government. We gratefully acknowledge the USDOE Office of Energy Efficiency and Renewable Energy, Office of Vehicle Technology for partially funding the reported work.

References

[1] Graboski, M. S., and McCormick, R. L., 1998, "Combustion of Fat and Vegetable Oil Derived Fuels in Diesel Engines," Prog. Energy Combust. Sci., **24**(2), pp. 125–164.
[2] McCormick, R. L., Williams, A., Ireland, J., Brimhall, M., and Hayes, R. R., 2006, "Effects of Biodiesel Blends on Vehicle Emissions," National Renewable Energy Laboratory (NREL), Golden, CO, Report No. NREL/MP–540-40554.
[3] Giakoumis, E. G., Rakopoulos, C. D., Dimaratos, A. M., and Rakopoulos, D. C., 2012, "Exhaust Emissions of Diesel Engines Operating Under Transient Conditions With Biodiesel Fuel Blends," Prog. Energy Combust. Sci., **38**(5), pp. 691–715.
[4] Lapuerta, M., Armas, O., and Rodríguez-Fernández, J., 2008, "Effect of Biodiesel Fuels on Diesel Engine Emissions," Prog. Energy Combust. Sci., **34**(2), pp. 198–223.
[5] Knothe, G., 2010, "Biodiesel and Renewable Diesel: A Comparison," Prog. Energy Combust. Sci., **36**(3), pp. 364–373.
[6] Feng, Q., Jalali, A., Fincham, A. M., Wang, Y. L., Tsotsis, T. T., and Egolfopoulos, F. N., 2012, "Soot Formation in Flames of Model Biodiesel Fuels," Combust. Flame, **159**(5), pp. 1876–1893.
[7] Agarwal, A. K., 2007, "Biofuels (Alcohols and Biodiesel) Applications as Fuels for Internal Combustion Engines," Prog. Energy Combust. Sci., **33**(3), pp. 233–271.
[8] Gill, S. S., Tsolakis, A., Dearn, K. D., and Rodríguez-Fernández, J., 2011, "Combustion Characteristics and Emissions of Fischer-Tropsch Diesel Fuels in IC Engines," Prog. Energy Combust. Sci., **37**(4), pp. 503–523.
[9] Murugesan, A., Umarani, C., Chinnusamy, T., Krishnan, M., Subramanian, R., and Neduzchezhain, N., 2009, "Production and Analysis of Bio-Diesel From Non-Edible Oils—A Review," Renewable Sustainable Energy Rev., **13**(4), pp. 825–834.
[10] Tiwari, A. K., Kumar, A., and Raheman, H., 2007, "Biodiesel Production From Jatropha Oil (Jatropha Curcas) With High Free Fatty Acids: An Optimized Process," Biomass Bioenergy, **31**(8), pp. 569–575.
[11] Banković-Ilić, I. B., Stamenković, O. S., and Veljković, V. B., 2012, "Biodiesel Production From Non-Edible Plant Oils," Renewable Sustainable Energy Rev., **16**(6), pp. 3621–3747.
[12] Achten, W. M. J., Verchot, L., Franken, Y. J., Mathijs, E., Singh, V. P., Aerts, R., and Muys, B., 2008, "Jatropha Bio-Diesel Production and Use," Biomass Bioenergy, **32**(12), pp. 1063–1084.
[13] Nabi, M. N., Hoque, S. M. N., and Akhter, M. S., 2009, "Karanja (Pongamia Pinnata) Biodiesel Production in Bangladesh, Characterization of Karanja Biodiesel and Its Effect on Diesel Emissions," Fuel Process. Technol., **90**(9), pp. 1080–1086.
[14] Agarwal, A. K., and Dhar, A., 2009, "Performance, Emission and Combustion Characteristics of Jatropha Oil Blends in a Direct Injection CI Engine," SAE Technical Paper No. 2009-01-0947.
[15] Sahoo, P. K., and Das, L. M., 2009, "Combustion Analysis of Jatropha, Karanja and Polanga Based Biodiesel as Fuel in a Diesel Engine," Fuel, **88**(6), pp. 994–999.
[16] Ganapathy, T., Gakkhar, R. P., and Murugesan, K., 2011, "Influence of Injection Timing on Performance, Combustion and Emission Characteristics of Jatropha Biodiesel Engine," Appl. Energy, **88**(12), pp. 4376–4386.
[17] Dhar, A., and Agarwal, A. K., 2014, "Performance, Emissions and Combustion Characteristics of Karanja Biodiesel in a Transportation Engine," Fuel, **119**(3), pp. 70–80.
[18] Sequera, A. J., Parthasarathy, R. N., and Gollahalli, S. R., 2011, "Effects of Fuel Injection Timing in the Combustion of Biofuels in a Diesel Engine at Partial Loads," ASME J. Energy Resour. Technol., **133**(2), p. 022203.
[19] Maurya, R. K., and Agarwal, A. K., 2105, "Combustion and Emission Characterization of *n*-Butanol Fueled HCCI Engine," ASME J. Energy Resour. Technol., **137**(1), p. 011101.
[20] McCormick, R. L., and Westbrook, S. R., 2009, "Storage Stability of Biodiesel and Biodiesel Blends," Energy Fuels, **128**(1), pp. 690–698.
[21] Monyem, A., and Van Gerpen, J. H., 2001, "The Effect of Biodiesel Oxidation on Engine Performance and Emissions," Biomass Bioenergy, **20**(4), pp. 317–325.
[22] Dunn, R. O., 2002, "Effect of Oxidation Under Accelerated Conditions on Fuel Properties of Methyl Soyate (Biodiesel)," J. Am. Oil Chem. Soc., **79**(9), pp. 915–920.
[23] Ramírez, A. I., Aggarwal, S. K., Som, S., Rutter, T. P., and Longman, D. E., 2014, "Effects of Blending a Heavy Alcohol ($C_{20}H_{40}O$ With Diesel in a Heavy-Duty Compression-Ignition Engine," Fuel, **136**, pp. 89–102.
[24] Ramirez, A., Som, S., Aggarwal, S. K., Kastengren, A., El-Hannouny, E., Longman, D., and Powell, C., 2009, "Quantitative X-Ray Measurements of High-Pressure Fuel Sprays From a Production Heavy Duty Diesel Injector," Exp. Fluids, **47**(1), pp. 119–134.
[25] Longman, D., 2006, "In-Cylinder Injection of Oxygen-Enriched Air to Educe Diesel Engine Exhaust Emissions," M.S. thesis, Department of Mechanical and Industrial Engineering, University of Illinois at Chicago, Chicago, IL.
[26] AVL, 2015, "Instrumentation and Test Systems," AVL LIST GmbH. Graz. Austria, https://www.avl.com/its

[27] Ciatti, S. A., Miers, S. A., and Ng, H. K., 2005, "Influence of EGR on Soot/NOx Production in a Light-Duty Diesel Engine," ASME Paper No. ICEF2005-1327.
[28] Som, S., Longman, D. E., Ramírez, A. I., and Aggarwal, S. K., 2010, "A Comparison of Injector Flow and Spray Characteristics of Biodiesel With Petrodiesel," Fuel, **89**(12), pp. 4014–4024.
[29] Assanis, D. N., Filipi, Z. S., Fiveland, S. B., and Syrimis, M. A., 2003, "Predictive Ignition Delay Correlation Under Steady-State and Transient Operation of a Direct Injection Diesel Engine," ASME J. Eng. Gas Turbines Power, **125**(2), pp. 450–457.
[30] Agarwal, A. K., Srivastava, D. K., Dhar, A., Maurya, R. K., Shukla, P. C., and Singh, A. P., 2013, "Effect of Fuel Injection Timing and Pressure on Combustion, Emissions and Performance Characteristics of a Single Cylinder Diesel Engine," Fuel, **111**, pp. 374–383.
[31] Agarwal, A. K., Srivastava, D. K., Dhar, A., Maurya, R. K., Shukla, P. C., and Singh, A. P., 2013, "Effect of Fuel Injection Timing and Pressure on Combustion, Emissions and Performance Characteristics of a Single Cylinder Diesel Engine," Fuel, **111**, pp. 374–383.
[32] Schönborn, A., Ladommatos, N., Williams, J., Allen, R., and Rogerson, J., 2009, "The Influence of Molecular Structure of Fatty Acid Monoalkyl Esters on Diesel Combustion," Combust. Flame, **156**(7), pp. 1396–1412.
[33] Benjumea, P., Agudelo, J. R., and Agudelo, A. F., 2011, "Effect of the Degree of Unsaturation of Biodiesel Fuels on Engine Performance," Combust. Charact. Emiss., Energy Fuel, **25**(1), pp. 77–85.
[34] Garner, S., and Brezinsky, K., 2011, "Biologically Derived Diesel Fuel and NO Formation: An Experimental and Chemical Kinetic Study, Part 1," Combust. Flame., **158**(12), pp. 2289–2301.
[35] Garner, S., Dubois, T., Togbe, C., Chaumeix, N., Dagaut, P., and Brezinsky, K., 2011, "Biologically Derived Diesel Fuel and NO Formation, Part 2: Model Development and Extended Validation," Combust. Flame, **158**(12), pp. 2302–2313.
[36] Han, X., Aggarwal, S. K., and Brezinsky, K., 2013, "On the Effect of Unsaturated Bond on NO_x and PAH Formation in n-Heptane and 1-Heptene Triple Flames," Energy Fuel, **27**(1), pp. 537–548.
[37] Fu, X., Han, X., Brezinsky, K., and Aggarwal, S. K., 2013, "Effect of Fuel Molecular Structure and Premixing on Soot Emissions From n-Heptane and 1-Heptene Flames," Energy Fuel, **27**(10), pp. 6262–6272.
[38] Mistri, G. K., 2015, "Performance and Emission Investigation of Jatropha and Karanja Biodiesels an a Single-Cylinder Compression-Ignition Engine With Optical Imaging," M.S. thesis, Department of Mechanical and Industrial Engineering, University of Illinois at Chicago, Chicago, IL.
[39] Desmira, N., Kitagawa, K., and Gupta, A. K., 2014, "Hydroxyl and Nitric Oxide Distribution in Waste Rice Bran Biofuel-Octanol Flames," ASME J. Energy Resour. Technol., **136**(1), p. 014501.
[40] Ban-Weiss, G. A., Chen, J. Y., Buchholz, B. A., and Dibble, R. W., 2007, "A Numerical Investigation into the Anomalous Slight NO_x Increase When Burning Biodiesel; A New (Old) Theory," Fuel Processing Technol, **88**(7): 659–667.